Fluorine-doped tin oxides for mid-infrared plasmonics

Farnood Khalilzadeh-Rezaie,[1] Isaiah O. Oladeji,[2] Justin W. Cleary,[3] Nima Nader,[3,4] Janardan Nath,[1] Imen Rezadad,[1] and Robert E. Peale[1,*]

[1]Department of Physics, University of Central Florida, Orlando, FL 32816, USA
[2]SISOM Thin Films LLC, Orlando, FL 32805, USA
[3]Air Force Research Laboratory, Sensors Directorate, Wright-Patterson Air Force Base, OH 45433, USA
[4] Solid State Scientific Corporation, Nashua, NH 03060, USA
[*]Robert.Peale@ucf.edu

Abstract: Fluorine-doped tin oxides (FTO) were investigated for infrared plasmonic applications. Nano-crystalline FTO thin films were grown by the SPEED chemical-spray deposition method. Complex permittivity spectra were measured from 1.6 to 12 μm wavelength. These spectra were used to calculate materials parameters, which compared well with values from transport measurements, and to predict characteristics of surface plasmon polaritons (SPP). Reflectivity spectra for lamellar FTO gratings revealed SPP coupling resonances in good agreement with predictions. The FTO film studied here is well suited for plasmonic applications in the important 3-5 μm wavelength range.

OCIS codes: (240.6680) Surface plasmons, (130.3060) Infrared, (160.4670) Optical materials, (250.5403) Plasmonics, (280.4788) Optical sensing and sensors.

References and links

1. A. S. Barker, Jr., "Optical measurements of surface plasmons in gold," Phys. Rev. B **8**(12), 5418–5426 (1973).
2. H. Raether, "Dispersion relation of surface plasmons on gold and silver gratings," Opt. Commun. **42**(4), 217–222 (1982).
3. Z. Schlesinger and A. Sievers, "IR surface plasmon attenuation coefficients for Ag and Au films," Solid State Commun. **43**(9), 671–673 (1982).
4. J. W. Cleary, G. Medhi, M. Shahzad, I. Rezadad, D. Maukonen, R. E. Peale, G. D. Boreman, S. Wentzell, and W. R. Buchwald, "Infrared surface polaritons on antimony," Opt. Express **20**(3), 2693–2705 (2012).
5. F. Khalilzadeh-Rezaie, C. W. Smith, J. Nath, N. Nader, M. Shahzad, J. W. Cleary, I. Avrutsky, and R. E. Peale, "Infrared surface polaritons on bismuth," J. Nanophotonics **9**(1), 093792 (2015).
6. R. Soref, R. E. Peale, and W. Buchwald, "Longwave plasmonics on doped silicon and silicides," Opt. Express **16**(9), 6507–6514 (2008).
7. J. Cleary, R. Peale, D. Shelton, G. Boreman, C. Smith, M. Ishigami, R. Soref, A. Drehman, and W. Buchwald, "IR permittivities for silicides and doped silicon," JOSA B **27**(4), 730–734 (2010).
8. M. Shahzad, G. Medhi, R. E. Peale, W. R. Buchwald, J. W. Cleary, R. Soref, G. D. Boreman, and O. Edwards, "Infrared surface plasmons on heavily doped silicon," J. Appl. Phys. **110**(12), 123105 (2011).
9. R. Soref, J. Hendrickson, and J. W. Cleary, "Mid- to long-wavelength infrared plasmonic-photonics using heavily doped n-Ge/Ge and n-GeSn/GeSn heterostructures," Opt. Express **20**(4), 3814–3824 (2012).
10. G. V. Naik, J. Kim, and A. Boltasseva, "Oxides and nitrides as alternative plasmonic materials in the optical range [Invited]," Opt. Mater. Express **1**(6), 1090–1099 (2011).
11. A. Boltasseva, "Empowering plasmonics and metamaterials technology with new material platforms," MRS Bull. **39**(05), 461–468 (2014).
12. P. R. West, S. Ishii, G. V. Naik, N. K. Emani, V. M. Shalaev, and A. Boltasseva, "Searching for better plasmonic materials," Laser Photonics Rev. **4**(6), 795–808 (2010).
13. A. Boltasseva and H. A. Atwater, "Materials science. Low-loss plasmonic metamaterials," Science **331**(6015), 290–291 (2011).
14. S. Law, D. C. Adams, A. M. Taylor, and D. Wasserman, "Mid-infrared designer metals," Opt. Express **20**(11), 12155–12165 (2012).
15. S. Law, L. Yu, and D. Wasserman, "Epitaxial growth of engineered metals for mid-infrared plasmonics," J. Vac. Sci. Technol. B **31**(3), 03C121 (2013).
16. E. Krivoy, A. Vasudev, H. P. Nair, V. D. Dasika, R. Synowicki, R. Salas, S. J. Maddox, M. Brongersma, and S. Bank, "Tunable, epitaxial, semimetallic films for plasmonics," in *CLEO 2013,* OSA Technical Digest (Optical Society of America, 2013), paper QTu1B. 7.

17. S. Law, V. Podolskiy, and D. Wasserman, "Towards nano-scale photonics with micro-scale photons: the opportunities and challenges of mid-infrared plasmonics," Nanophotonics **2**(2), 103–130 (2013).
18. G. V. Naik, V. M. Shalaev, and A. Boltasseva, "Alternative plasmonic materials: beyond gold and silver," Adv. Mater. **25**(24), 3264–3294 (2013).
19. M. Noginov, L. Gu, J. Livenere, G. Zhu, A. Pradhan, R. Mundle, M. Bahoura, Y. A. Barnakov, and V. Podolskiy, "Transparent conductive oxides: Plasmonic materials for telecom wavelengths," Appl. Phys. Lett. **99**(2), 021101 (2011).
20. S. Franzen, C. Rhodes, M. Cerruti, R. W. Gerber, M. Losego, J.-P. Maria, and D. E. Aspnes, "Plasmonic phenomena in indium tin oxide and ITO-Au hybrid films," Opt. Lett. **34**(18), 2867–2869 (2009).
21. G. V. Naik, J. Liu, A. V. Kildishev, V. M. Shalaev, and A. Boltasseva, "Demonstration of Al:ZnO as a plasmonic component for near-infrared metamaterials," Proc. Natl. Acad. Sci. U.S.A. **109**(23), 8834–8838 (2012).
22. L. Dominici, F. Michelotti, T. M. Brown, A. Reale, and A. Di Carlo, "Plasmon polaritons in the near infrared on fluorine doped tin oxide films," Opt. Express **17**(12), 10155–10167 (2009).
23. H. L. Hartnagel, A. Dawar, A. Jain, and C. Jagadish, *Semiconducting Transparent Thin Films* (Institute of Physics Pub. Bristol, , 1995).
24. S. Franzen, "Surface plasmon polaritons and screened plasma absorption in indium tin oxide compared to silver and gold," J. Phys. Chem. C **112**(15), 6027–6032 (2008).
25. C. Rhodes, M. Cerruti, A. Efremenko, M. Losego, D. Aspnes, J.-P. Maria, and S. Franzen, "Dependence of plasmon polaritons on the thickness of indium tin oxide thin films," J. Appl. Phys. **103**(9), 093108 (2008).
26. M. Abb, P. Albella, J. Aizpurua, and O. L. Muskens, "All-optical control of a single plasmonic nanoantenna-ITO hybrid," Nano Lett. **11**(6), 2457–2463 (2011).
27. S. H. Brewer and S. Franzen, "Optical properties of indium tin oxide and fluorine-doped tin oxide surfaces: correlation of reflectivity, skin depth, and plasmon frequency with conductivity," J. Alloys Compd. **338**(1-2), 73–79 (2002).
28. F. Khalilzadeh-Rezaie, I. O. Oladeji, G. T. Yusuf, J. Nath, N. Nader, S. Vangala, J. W. Cleary, W. V. Schoenfeld, and R. E. Peale, "Optical and electrical properties of tin oxide-based thin films prepared by streaming process for electrodeless electrochemical deposition," in *MRS Proceedings* (Cambridge Univ Press, 2015), Vol 1805, pp. mrss15–2136423.
29. I. O. Oladeji, "Film growth system and method," (U.S. Patent No. 7,793,611, 2010).
30. F. Wooten, *Optical Properties of Solids* (Academic Press, 1972).
31. L. D. Landau, E. M. Lifshitz, and L. P. Pitaevskii, *Electrodynamics of Continuous Media 2nd edition* (Elsevier Butterworth Heinemann, 1984), section 77.
32. R. Heintz, *Surface Plasmons on Smooth and Rough Surfaces and on Gratings*, (Springer, 1986).
33. P. Patnaik, *Handbook of inorganic chemicals* (McGraw-Hill New York, 2003).
34. A. Rakhshani, Y. Makdisi, and H. Ramazaniyan, "Electronic and optical properties of fluorine-doped tin oxide films," J. Appl. Phys. **83**(2), 1049–1057 (1998).
35. J. W. Cleary, G. Medhi, R. E. Peale, and W. R. Buchwald, "Long-wave infrared surface plasmon grating coupler," Appl. Opt. **49**(16), 3102–3110 (2010).
36. J. W. Cleary, W. H. Streyer, N. Nader, S. Vangala, I. Avrutsky, B. Claflin, J. Hendrickson, D. Wasserman, R. E. Peale, W. Buchwald, and R. Soref, "Platinum germanides for mid- and long-wave infrared plasmonics," Opt. Express **23**(3), 3316–3326 (2015).

1. Introduction

Surface plasmon polaritons (SPPs) are inhomogeneous electromagnetic waves that are bound to the surface of a conductor, in which traveling density waves of free electrons are the sources of the SPP fields. Tight confinement of electromagnetic (EM) energy, the primary virtue of SPPs for plasmonic device applications, requires plasma frequencies for the conductor near the intended operational frequency. Many studies of SPPs have been conducted for propagating plasmons on the surface of good metals in the visible spectrum [1, 2]. Some studies have been published about IR SPPs on metals [3], semimetals [4, 5], doped-semiconductors [6–9], and other materials [10–22].

Noble metals such as Au and Ag are traditional SPP hosts with plasma frequencies in the visible part of the spectrum. Such fail to tightly confine infrared SPPs [6]. Particularly for sensing applications, there is a need for new SPP hosts with infrared (IR) plasma frequencies. Especially attractive would be ones whose optical properties can be adjusted in fabrication or actively tuned post fabrication [10–12], and which have low dissipation [13–16]. Review of IR plasmonic materials can be found in [17, 18].

Transparent conducting oxides (TCOs) are potentially useful SPP host materials [19]. Examples include indium tin oxide (ITO) [20], aluminum-doped zinc oxide (AZO) [21], and fluorine-doped tin oxide (FTO) [22]. Lower carrier concentrations ($10^{20\text{-}22}$ cm^{-3}) than for

metals (10^{23} cm^{-3}) puts their plasma frequencies in the IR region. TCOs can potentially host and guide SPPs with relatively low loss and fairly high mode confinement [19].

This paper reports an investigation of SPP properties for FTO films. Integration of FTO into optoelectronic devices may be easier than for Ag and Au [12, 23]. Though experimental and theoretical literature on TCO plasmonics is growing, particularly for ITO [24, 25], AZO [21] and ITO/metal hybrids [20, 26], little work has been done on FTO, except as near-IR attenuated total reflectance (ATR) couplers [22] and investigation of commercial FTO thin-films by Fourier transform infrared (FTIR) spectroscopy [27]. A motivation for the present work is our specific and advantageous means of FTO growth, which allows perfect conformal coating of lamellar gratings cut in silicon substrates. The growth method is a variant of chemical bath deposition known as Streaming Process for Electrodeless Electrochemical Deposition (SPEED), which was developed by SISOM Thin Films LLC [28, 29].

2. Theoretical considerations

The long-wavelength permittivity of a conductor can usually be described by the Drude free electron model [30]

$$\varepsilon = \varepsilon_\infty - \frac{(\omega_p/\omega)^2}{1+i/\omega\tau}, \omega_p^2 = \frac{ne^2}{m\,\varepsilon_0}, \tag{1}$$

where τ is the relaxation time, and ε_∞ is the real part of the permittivity well above the plasma frequency, which is defined in SI units with n, e and m as charge density, electron charge, and electron mass, respectively. If $\omega\tau \gg 1$, ε is real, and the permittivity changes sign at $\omega = \omega_p/\sqrt{\varepsilon_\infty}$. The real and imaginary parts of Eq. (1) are

$$\varepsilon' = \varepsilon_\infty - \frac{(\omega_p/\omega)^2}{1+(\omega\tau)^{-2}} \tag{2}$$

$$\varepsilon'' = \frac{(\omega_p/\omega)^2\,\omega\tau}{1+(\omega\tau)^{-2}} \tag{3}$$

At sufficiently long wavelengths for which $\omega\tau \ll 1$, Eq. (3) becomes linear in wavelength. However, for conductors at sufficiently long wavelength, we also expect [31]

$$\varepsilon'' = \frac{\sigma}{\varepsilon_0\omega} \tag{4}$$

which allows a determination of DC conductivity σ from the far-IR ε'' spectrum. Comparison of Eqs. (3) and (4) in the long-wave limit gives the relation

$$\sigma = \varepsilon_0\omega_p^2\tau \tag{5}$$

providing a useful check on obtained parameter values, since σ can be determined from DC transport measurements such as Hall effect and 4-point probe.

SPP field confinement and propagation length are metrics that determine if a plasmon host is useful for plasmonic applications. The 1/e SPP field penetration depth from the interface of conductor/dielectric into either the conductor (c) or dielectric (d) side is

$$L_{d,c} = \left[\frac{2\pi}{\lambda}\text{Re}\left(\sqrt{\frac{-\varepsilon_{d,c}^2}{\varepsilon_d+\varepsilon_c}}\right)\right]^{-1} \tag{6}$$

where ε_c and ε_d are the complex permittivity of the conductor and the dielectric, respectively. The characteristic SPP intensity propagation length is

$$L_x = \left[2 \, \mathrm{Im}(\mathrm{k}_{SPP}) \right]^{-1} \qquad (7)$$

where the SPP wavevector is

$$k_{SPP} = \frac{2\pi}{\lambda} \sqrt{\frac{\varepsilon_d \varepsilon_c}{\varepsilon_d + \varepsilon_c}} \qquad (8)$$

The 1/e electric-field penetration depth for electromagnetic waves (skin depth) incident on a conductor is

$$\delta = \left(\frac{2\pi}{\lambda} \mathrm{Im}(\sqrt{\varepsilon}) \right)^{-1} \qquad (9)$$

This value is useful in determining whether deposited films are optically thick for purposes of ellipsometry and SPP grating couplers. We expect $\delta \approx L_c$ on the basis of physical intuition, even though their expressions appear quite different.

The function of a grating coupler is to add horizontal components of momentum to the incident light, which allows coupling to the horizontally propagating SPPs. SPP excitation on gratings is expected for the TM-polarized light (E-field normal to grating grooves) when the momentum conservation condition is satisfied [32], namely

$$\pm \mathrm{Re}\left(k_{SPP} \right) = \frac{2\pi}{\lambda} \left[\sin(\theta) + \frac{m\lambda}{p} \right] \qquad (10)$$

In Eq. (10), m is an integer of either sign and p is the grating period.

3. Experimental details

FTO thin films were deposited onto Si (100) substrates by the SPEED process described in [28, 29]. The ratio of fluorine to tin was kept at 20% in chemical solutions while the films were deposited at temperatures near 500 °C in air [28]. Film morphology was characterized by scanning electron microscopy (SEM). Resistivity, mobility, and carrier concentration were determined from Hall measurements (MMR technologies) at room temperature in a Van der Pauw four-point probe configuration using indium contacts and a magnetic induction of 0.65 T. Variable angle spectroscopic ellipsometer (IR-Vase by J. A. Woollam) from 1.5 to 12 μm was used to determine the complex permittivity spectrum.

Lamellar Si gratings were fabricated by photolithography and deep-reactive ion etching (DRIE, fluorine chemistry), then conformally coated with FTO by SPEED. Finished gratings were characterized by SEM and by step profilometry. For cross section SEM, the samples were cleaved across the grating bars, potted in epoxy, and mechanically polished.

Reflectivity spectra of FTO gratings for normal incidence ($\theta = 0$ in Eq. (10)) were collected using a Bruker Fourier transform spectrometer equipped with a Hyperion IR microscope. The objective was removed from the microscope to achieve a collimated beam on the sample at normal incidence. The spectral resolution was 4 cm^{-1}. Resources included a globar source, a KBr beam splitter, and a 77 K Mercury-Cadmium-Telluride (MCT) detector.

Angle-dependent specular reflectance of gratings was measured using a goniometer with motor-controlled rotational sample stage and detector arm (Huber). A LabView program controlled the sample's angle θ with respect to the incident laser beam, while reflection from the grating was recorded at 2θ angle by a detector on a concentric but independently controlled stage. A tunable quantum cascade laser (QCL, Daylight Solutions) with spectral resolution of 0.1 nm, tunable from 7.9 to 10.5 μm wavelength, and electronically-chopped at 1 kHz was incident on the grating in TM polarization. A mercury cadmium telluride (MCT) detector collected the reflected intensity, and a lock-in synchronously amplified the signal. A LabView program recorded the lock-in output as a function of incidence angle. Background

was characterized with a gold mirror in place of the grating. Reflectance is the ratio of grating and reference spectra.

4. Results

Figure 1 presents an SEM image of a SPEED-grown FTO film. The top surface of the film shows that it comprises a dense array of nanocrystals with observable facets. Crystallinity of the film is supported by the sharp peaks observed in x-ray diffraction [28]. The average grain size is less than 0.2 μm. Thus, very little scattering is expected at IR wavelengths.

Fig. 1. SEM image of SPEED-grown FTO film.

Figure 2 (a) presents complex permittivity spectra for a 250 nm-thick FTO film that had particularly high conductivity. These spectra provide much information about FTO optical and electrical properties, which is collected in Table 1. Firstly, we note that the real part of the permittivity ε' becomes negative beyond $\lambda \equiv \lambda_0 = 2.11$ μm, which is the region suitable for SPPs. Equations (2) and (3) were fit (dashed lines) to the complex permittivity spectrum to obtain the parameters ω_p, ε_∞, and τ. The quantity $\sqrt{\varepsilon_\infty}$ should equal the refractive index at frequencies well above those for which the dispersion due to free electrons is important. We find $\sqrt{\varepsilon_\infty} = 1.96$, which is much closer to the refractive index values (2.006 [33] and 2 [34]) that have been reported for SnO_2 in the visible range than is the value $\sqrt{\varepsilon_\infty} = 1.71$ obtained from [22], see Table 1. The obtained ω_p value is used to determine a value for the carrier concentration n (Table 1), which is very similar to the value determined from the data reported in [22]. Applying Eq. (4) to the linear part of the ε'' spectrum beyond ~6 μm wavelength, where the slope is 6.7 $μm^{-1}$, determines a value for the resistivity which is in good agreement with values from our Hall and 4-point probe measurements, Table 1. Our value for relaxation time can be used [27] to estimate the electron mobility $\mu = e\tau/m = 6.5$ cm^2/V-s, which agrees well with our value $\mu = 7.2$ cm^2/V-s from Hall measurements for the considered sample [28]. According to Eq. (5), ω_p can be found from resistivity and relaxation time. Using the optical and Hall values for ρ and τ give the same 1.85×10^{15} rad/s value for ω_p, which is within 4% of the value given in Table 1 from the full fit. All determined parameters collected in Table 1 are compared to values from [22] for a commercial FTO film

prepared by a different method. A future report will describe the dependence of the optical properties on growth temperature and doping concentration. The present paper highlights the best results achieved thus far on the most metallic of the FTO samples yet grown [28], as examples of the plasmonic potential for FTO.
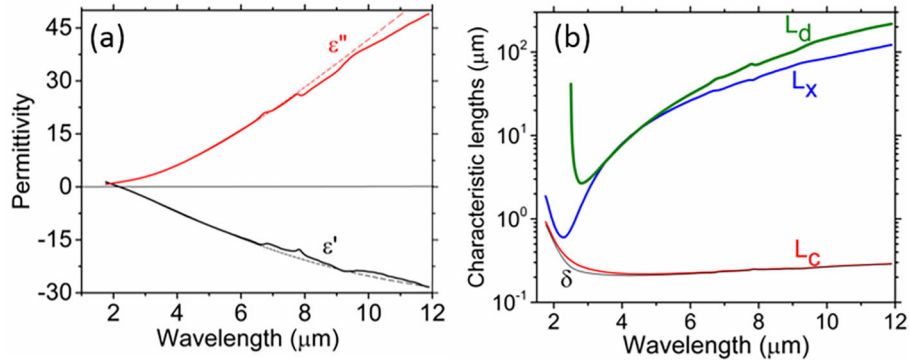

Fig. 2. (a) Infrared complex permittivity spectrum of SPEED-grown FTO film. The Drude fit is the dashed line. (b) Characteristic length spectra in FTO: SPP penetration depths into dielectric (L_d), conductor (L_c), IR skin depth (δ) and SPP intensity propagation length (L_x).

Figure 2 (b) presents calculated spectra for the characteristic lengths Eqs. (6), (7), and (9) when the dielectric is air with permittivity of unity. The optical penetration depth is comparable to our 250 nm film thickness throughout most of the spectrum, and in the near-IR the penetration exceeds the thickness. As expected, $\delta \approx L_c$.

Criteria for comparing the useful spectral range for plasmonic applications of different materials were suggested in [6]. These were that the penetration depth L_c of the SPP field into the dielectric (air) should be less than thrice the free space wavelength, and that the intensity propagation length should be at least twice the wavelength. From Fig. 2 (b) we see that these criteria are satisfied within the range $4 < \lambda < 5$ μm wavelength. In otherwords, the FTO film studied here appears well suited for mid-wave IR applications. We remind that the doping of FTO can be tailored to access the long-wave (thermal) IR portion of the spectrum, in principle.

For comparison, on the basis of the same criteria [6], different materials have different useful plasmonic spectral ranges. Using only available published L_d and L_x spectra based on *measured* permittivity values, we find the following useful spectral ranges, in order of increasing wavelength: Ag (< 2.3 μm) [35], silicides (1-7 μm) [7], $PtGe_2$ (2-7 μm) [36], Pt_2Ge_3 (2-15 μm) [36], Si with p = 10^{20} cm^{-3} (6-10 μm) [8], and Sb [11-20 μm] [4]. The semi-metal Bi does not satisfy the confinement criterion $L_d < 3\lambda$ at any wavelength from near to far IR [5]. For Si with p = 6 x 10^{19} cm^{-3}, there is no wavelength where both confinement and propagation criteria are satisfied simultaneously [8]. To apply the Ref [6]. criteria to doped epitaxial semiconductors [14–16] will require a calculation of yet-unpublished L_d and L_x spectra from the measured permittivities. According to the comparison above, only silicides, germanides, and FTO are suitable for plasmonic applications in the 3-5 μm wavelength range, and FTO fails to fully span it. On the other hand, SPEED-grown FTO has other advantages that may make it preferable, such as low-cost of deposition without vacuum and perfect conformal coating.

Table 1. Drude parameters for FTO films.

Paremeter	Thickness (nm)	λ_0 (μm)	ω_p (rad/s)	ε_∞	n (10^{21} cm^{-3})	τ (fs)	ρ(μΩ-cm) (ε''/Hall/4pt)
This work	250	2.11	1.78×10^{15}	3.85	0.997	3.69	895/800/970
Dominici et al. [22]	510	1.8	1.82×10^{15}	2.95	1.04	4.92	(690*/–/–)

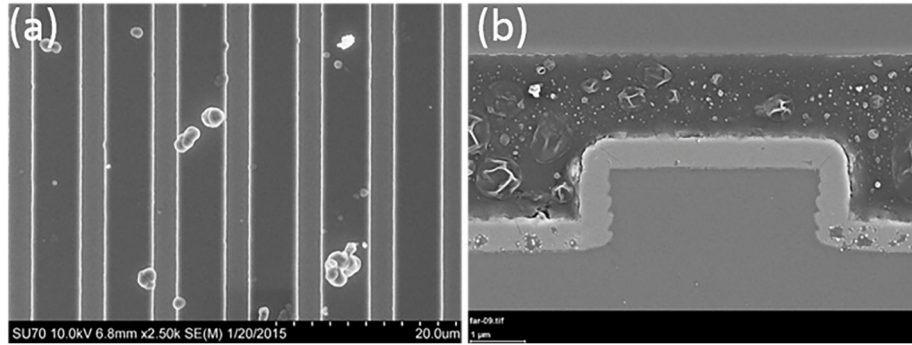*Value determined according to Eq. (5).

Fig. 3. Scanning electron microscope images of FTO-coated silicon lamellar grating. (a) Top view. (b) Side view. (The granular medium above the grating is the mounting epoxy used in polishing.)

Figure 3 presents SEM images in top view and cross section for an FTO grating with 7.5 μm period and 1.46 μm groove depth. The depth was confirmed by step profilometry. The photomask had a 50% duty cycle, and the finished FTO-coated grating has a 70% duty cycle. The cross-section shows that the SPEED process results in an exceptionally conformal FTO coating with uniform thickness on horizontal and vertical surfaces. The nanocrystals are so densely packed without voids, that none of the nanostructure seen in the Fig. 1 top view is evident in cross section.
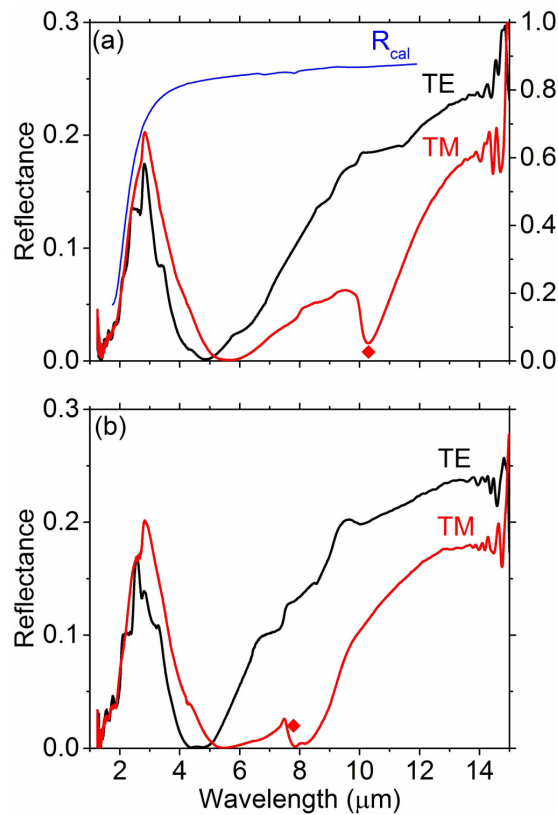

Fig. 4. Normal incidence reflectivity spectra for TM and TE polarizations normally incident on an FTO grating with (a) p = 10 μm (b) p = 7.5 μm. The R_{cal} curve in plot (a) gives the Fresnel reflectance calculated for unstructured FTO from the measured permittivity spectrum.

Figure 4 presents measured reflectivity spectra in TE and TM polarizations for two different grating periods. In TE polarization, no SPP should be excited. Since reflectivity calculated from the ε'' spectrum is featureless (Fig. 4 (a)), there should be no absorption bands related to the FTO itself. Nevertheless, we observe a broad minimum in TE reflectance from the gratings. We tentatively attribute this band to a Wood's anomaly of Rayleigh type. In other words, the power in the measured specular beam, which is the zeroth diffracted order, decreases when a new diffracted order enters the space above the grating. This condition is given from the grating equation [35] for normal incidence by $\lambda = p/m$, where for the gratings with 7.5 and 10 μm, the $m = 2$ Rayleigh features should be at 3.8 and 5 μm wavelength, respectively. These values agree roughly with the observed positions of the TE bands and with their relative positions for the different grating periods. That they are absent from the reflectivity of smooth FTO films (e.g. R_{cal}) is consistent with our interpretation. Such features were outside the range (8-10.5 μm) of the reflectivity spectra reported in our earlier studies of bismuth [5] and germanide [36] gratings.
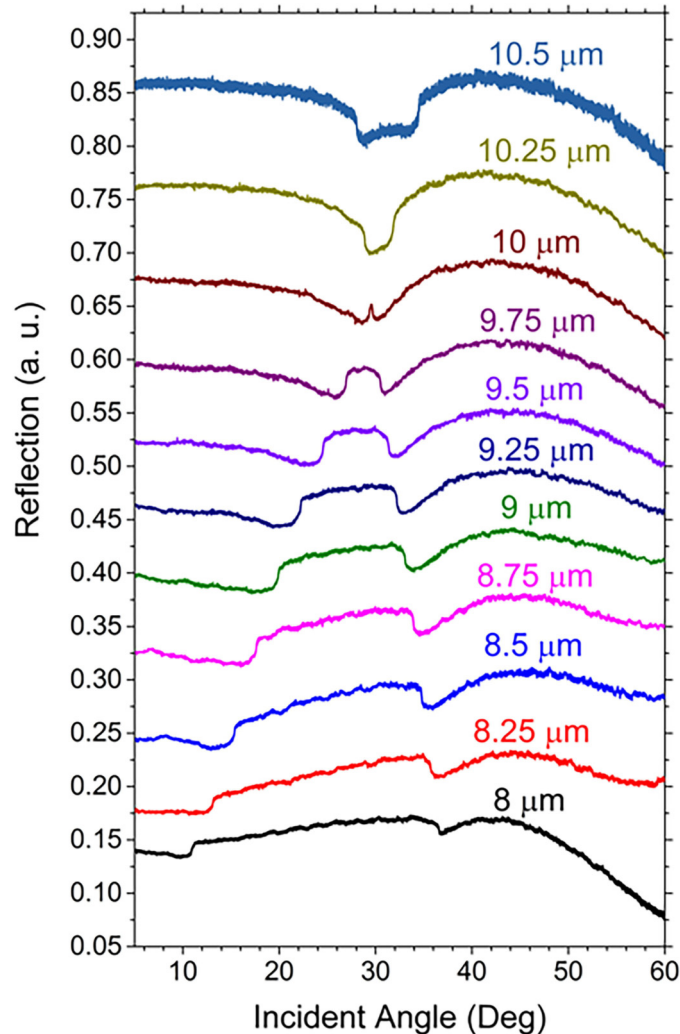

Fig. 5. Angular reflectance spectra for different wavelengths of TM-polarized incident beam.

In TM-polarization, new absorption bands appear at ~8 and 10.3 μm wavelength for 7.5 and 10 μm period gratings, respectively. Both wavelengths are slightly longer than the

corresponding grating period, which is expected from Eq. (10) with $m = 1$, since $\text{Re}[k_{SPP}]$ always exceeds $2\pi/\lambda$. Symbols give the expected wavelengths for absorption by SPP creation from Eq. (10). The agreement leads us to interpret the additional bands as being due to SPPs, thus demonstrating the generation of long-wave IR SPPs on FTO.

Figure 5 presents angular reflectance spectra of a FTO grating with 20 μm period for a number of different QCL wavelengths. The absorption features look very similar, appear at similar angles, and shift similarly with wavelength as those reported for SPP excitation on Ag gratings [35]. Thus, we identify these absorption features unambiguously as due to excitation of SPPs. The observed resonances in Fig. 5 are the $+1$ and -3 orders according to Eq. (10). They are over twice broader than those reported for Ag gratings [35], which is evidence of higher loss due to larger ε'' relative to ε'. On the other hand, infrared SPPs on FTO will have tighter confinement due to its smaller plasma frequency. The $m = -3$ resonances appear to be somewhat sharper than those for $m = +1$. Sharper resonances may be more useful for plasmonic applications.

5. Summary

Surface plasmon polaritons on fluorine-doped tin oxide films grown by SPEED were investigated in the near- to long-wave- IR spectral range. The complex permittivity spectrum was measured and used to determine the values of plasma frequency and relaxation time of FTO films. These Drude parameters were used to determine the resistivity and mobility values, which were compared to experimental values from transport measurements. The permittivity spectrum was used to predict SPP properties such as intensity propagation length, field penetration depths, and reflectivity. Normal-incidence reflectivity spectra of FTO-coated gratings revealed SPP excitation features that agreed accurately with predictions. The FTO film studied here would be suitable for plasmonic applications in the important 3-5 μm spectral range.

Acknowledgments